Tuning Brønsted Acidity by up to 12 pK_a Units in a Redox-Active Nanopore Lined with Multifunctional Metal Sites

Taro J. Jones,[‡] Kaitlyn G. Dutton,[‡†] Harender S. Dhattarwal, P. Thomas Blackburn, Richard C. Remsing,* Mark C. Lipke*

Department of Chemistry and Chemical Biology, Rutgers, The State University of New Jersey, 123 Bevier Road, Piscataway, New Jersey 08854, United States

ABSTRACT: Electrostatic interactions, hydrogen bonding, and solvation effects can alter the free energies of ionizable functional groups in proteins and other enclosed porous architectures, allowing these nanostructures to tune acid-base chemistry as needed to support specific functions. Herein, we expand on this theme to examine how metal sites (M = H_2, Zn^{II}, Co^{II}, Co^{I}) affect the pK_a of benzoic acid guests bound in discrete porphyrin nanoprisms (**M_3TriCage**), which were chosen as model systems for better understanding how porous metalloporphyrin electrocatalysts might influence H^+ transfer processes that are needed to support many important electrochemical reactions (e.g., reductions of H^+, O_2, or CO_2). Lewis acidic Co^{II} and Zn^{II} ions increase the Brønsted acidities of the guests by 4 and 8 pK_a units, respectively, while reduction of the Co^{II} sites to anionic Co^{I} sites produces an electrostatic potential that lowers acidity by ca. 4 units (8 units relative to the Co^{II} state). Lacking functional metal sites, **H_6TriCage** increases the acidity of the guests by just 2.5 pK_a units despite the 12+ charge of the host and contributions from other factors (hydrogen bonding, pore hydration) that might stabilize the deprotonated guests. Thus, the metal sites have dominant effects on acid-base chemistry in the **M_3TriCages**, providing a larger pK_a range (12.75 to ≥24.5 in CD_3CN) for an encapsulated acid than attained via other confinement effects in proteins and artificial porous materials.

Introduction.

The free energies of ions can be modified significantly by nanoconfinement (Scheme 1A),[1-7] giving rise to important influences on acid-base chemistry in proteins[3-5] and other 3D nanostructures.[1,6,7] For example, proteins control solvation,[3] Coulombic effects,[4] and hydrogen bonding[5] to stabilize or destabilize the ionized state of an acid-base pair, thereby tuning the pK_a of acidic groups[3d,4b,5c] as needed to support functions ranging from catalysis[4b,4c,5c] to proton pumping.[8] Strong control over acid-base chemistry has also been achieved in artificial porous structures,[6,7] such as metal-organic nanocages,[1,6] but these examples are often attributed primarily to Coulombic effects[6a-f] rather than the myriad of factors that modulate acidity in proteins.[3-5,9] Thus, in early examples from Raymond and Bergman (Scheme 1B),[6a-c] anionic nanocages were found to favor the binding of cationic guests,[6a] making guests easier to protonate and accelerating acid-catalyzed transformations inside these structures.[6b,c] Likewise, Fujita[6d] and Ward[6e,f] have each used cationic cages to promote base-catalyzed reactivity.[6d-f]

However, recent studies reveal more complex influences on acid-base chemistry in charged hosts. Hooley has reported enhanced acidities for ammonium cations in a positively charged nanocage, as is expected, but non-Coulombic effects must also contribute to this behavior since the sequential protonation of 12 amines led to progressively lower pK_a values even though charge balance was maintained by anion uptake.[6g] Gibb has also noted that the Coulombic influences of charged hosts can be modulated by hydrogen bonding, hydration, and other factors to determine the acidities of encapsulated guests.[7b] Given the complex range of possible influences on acid-base behavior in confined microenvironments,[3-9] there remains considerable room to better understand how hollow structures affect the free energies of protons and other charged species.

We became interested in this question in the context of redox-active porphyrin nanostructures[10,11] that have been used as electrocatalysts for reactions such as the reduction of CO_2 or O_2.[12,13] A variety of metalloporphyrin nanocages[12] and framework materials[13] have been examined in this regard, but these studies have rarely addressed[13d] how the active sites in these materials might affect charged intermediates and proton relay chains that are important for efficient turnover.[14] These questions are especially vexing because redox changes will alter the distribution of charge[11b] at the active sites during catalysis,[13b] further complicating the confinement effects described above. Thus, we identified (tmeda)Pt-linked porphyrin nanoprisms[11] (**M_3TriCages**, M = H_2, Co, Zn, Scheme 1C,D) as useful subjects for probing how protons and other ions[11b] are affected by confinement in redox-active 3D porphyrin assemblies.

We previously reported that **H_6TriCage** (also referred to herein as **TriCage**) binds a large cationic guest upon adding 1 e^- to each porphyrin unit (Scheme 1C),[11b] and we hypothesized that similar electrostatic effects might be seen upon reduction of **Co_3TriCage** to its zwitterionic *tris*-Co^{I} state.[11c]

https://doi.org/10.26434/chemrxiv-2024-4w50c-v2 **ORCID:** https://orcid.org/0000-0003-0035-4565 Content not peer-reviewed by ChemRxiv. **License:** CC BY-NC-ND 4.0

Scheme 1. The effects of nanoconfinement on Brønsted acidity and other chemistry involving charged species.

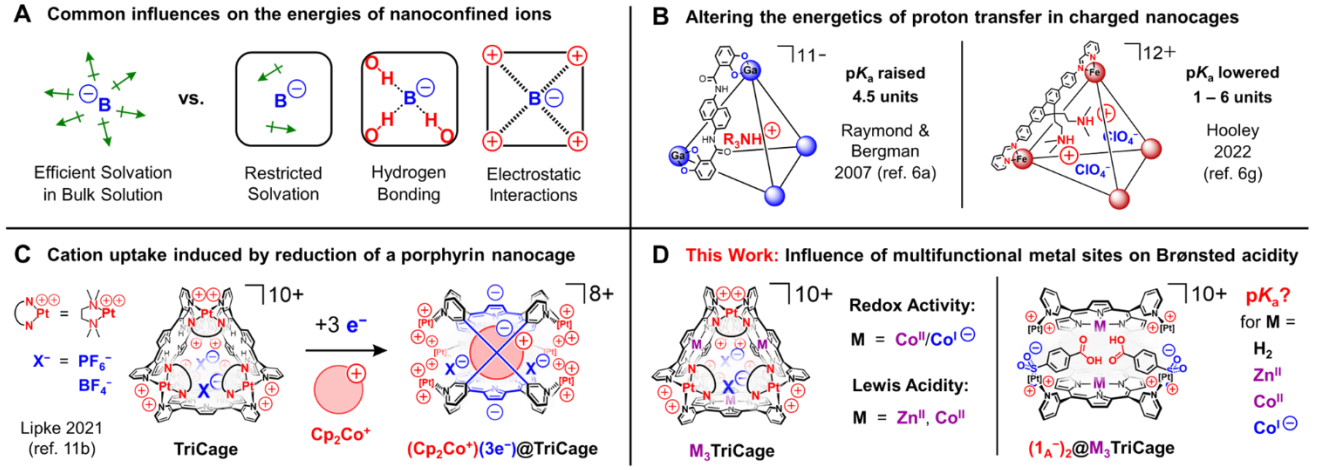

To measure the impact on proton transfer equilibria, the anion-binding ability of the TriCages was used to install two 4-sulfanatobenzoic acid guests (**1**$_A^-$, Scheme 1D) in each cage, following our observation that *p*-toluenesulfonate (**2**$^-$) binds strongly in **TriCage** ($K_a \approx 10^{7.5}$ M^{-1} in CD_3CN).[11d] Remarkably, the resulting complexes have acidities that are varied across a larger pK_a range (12.75 to ≥24.5 in CD_3CN) than those achieved in proteins and other nanocages,[3-9,15] even though Coulombic effects, hydrogen bonding, and hydration have only small to moderate influences on acidities in the TriCages. Instead, as described herein, the redox-active and/or Lewis acidic Co and Zn sites have dominant effects on increasing or decreasing the acidities of the guests, revealing the unique influences of these metalloporphyrin nanocages on acid-base chemistry.

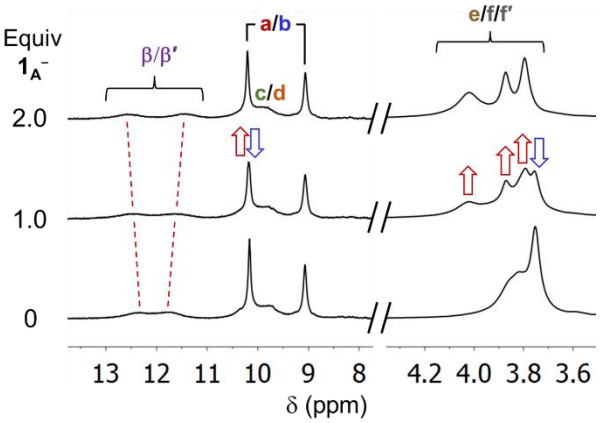

Figure 1. Truncated ^{1}H NMR spectra (500 MHz, CD_3CN, 25 °C) acquired during addition of **1**$_A^-$ to **Co$_3$TriCage**. Note that labels of signals correspond to those indicated in Scheme 2, and different scaling is used in each region of the spectra displayed.

Results and Discussion.

Complexation of acid/base functionalized guests. ^{1}H NMR spectroscopy was used to examine the encapsulation of 4-sulfanatobenzoic acid (**1**$_A^-$) and its conjugate base 4-sulfanatobenzoate (**1**$_B^{2-}$) by the TriCages in CD_3CN (Scheme 2). For all three **M$_3$TriCage** derivatives, addition of 2 equiv **1**$_A^-$ (as its TBA$^+$ salt) resulted in disappearance of the signals of the empty host and appearance of a new set of signals corresponding to a 1:2 host-guest complex (Figures 1, S27, and S39). ESI(+)-HRMS further confirmed the formation of **(1**$_A^-$**)$_2$@TriCage** and **(1**$_A^-$**)$_2$@Co$_3$TriCage** (Figures S53 and S56). However, the latter mass spectrum indicated partial deprotonation of the bound guests, and attempts to observe **(1**$_A^-$**)$_2$Zn$_3$TriCage** showed only the doubly deprotonated complex **(1**$_B^{2-}$**)$_2$@Zn$_3$TriCage**, providing an early indication that the acidity of **1**$_A^-$ is enhanced in the metallated derivatives of **TriCage** (*vide infra*).

Quantitative binding of **1**$_A^-$ in the TriCages is consistent with the strong 1:2 association of **2**$^-$ in **TriCage**. However, while **2**$^-$ binds noncooperatively, **1**$_A^-$ associates with positive cooperativity. Hence, an equimolar mixture of **1**$_A^-$ and **Co$_3$TriCage** displays an NMR spectrum consistent with the empty host combined in equal amounts with the 1:2 complex (Figure 1). Likewise, titration of **TriCage** and **Zn$_3$TriCage** with **1**$_A^-$ results in direct conversion of these hosts to their 1:2 complexes, with only small signals potentially corresponding to a 1:1 complex observed during the experiment (Figures S28 and S40). Mass spectrometry of a 1:1 mixture of **TriCage** and **1**$_A^-$ (Figure S54) also supports the cooperativity of guest binding, showing the 1:1 complex as a minor component (~8 %) of the sample relative to the empty host and 1:2 complex. The cooperative binding of **1**$_A^-$ was initially attributed to hydrogen-bonding between the guests, but as discussed below, traces of water were found to promote this cooperativity, suggesting that more complex factors underly this behavior.

In contrast to **1**$_A^-$, the deprotonated guest **1**$_B^{2-}$ shows considerable variation in its interactions with the different **M$_3$TriCage** derivatives. Addition of 1 equiv **1**$_B^{2-}$ to **Co$_3$TriCage** resulted in complete disappearance of the ^{1}H NMR signals of the empty host, and the appearance of several new signals that were shifted considerably from those of **Co$_3$TriCage** (Figure 2A). Most notably, the two porphyrin β CH resonances are split into three similarly sized groups of broad signals, one group resembling those of the empty host (δ 11 – 13 ppm) while two others are shifted downfield to ranges of δ 13.8 – 15.8 and 16.6 – 19.9 ppm. These latter signals are reminiscent of how the β CH signals appear when simple

https://doi.org/10.26434/chemrxiv-2024-4w50c-v2 **ORCID:** https://orcid.org/0000-0003-0035-4565 Content not peer-reviewed by ChemRxiv. **License:** CC BY-NC-ND 4.0

Scheme 2. Host-guest chemistry established for association of 1_A^- or 1_B^{2-} inside M_3TriCage (M = Co, Zn, H_2) in CD_3CN.

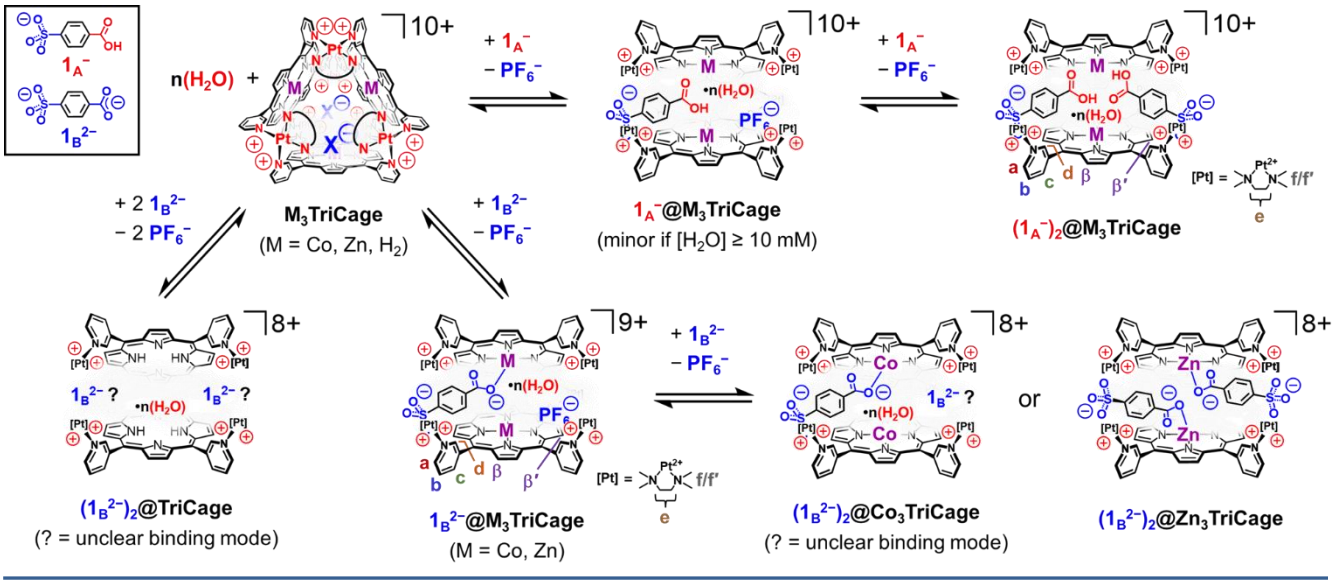

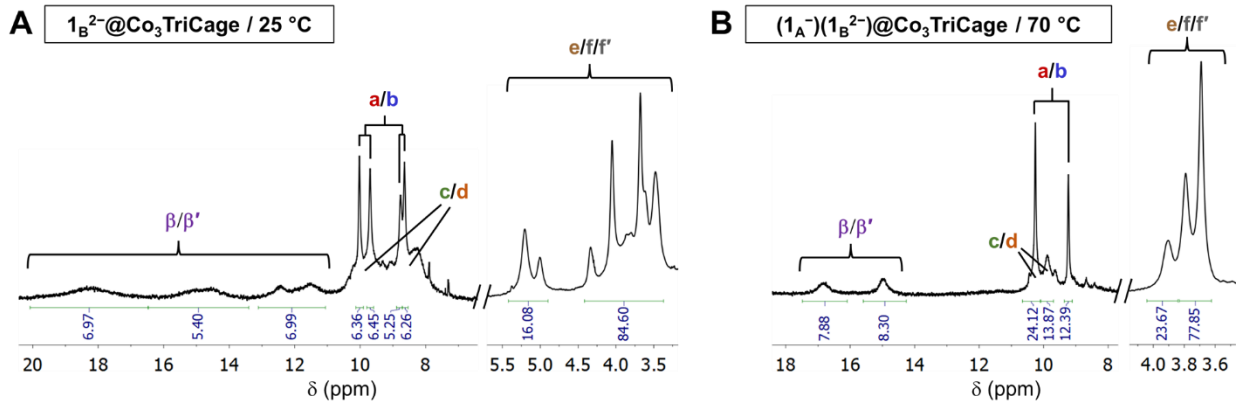

Figure 2. (A) Truncated ^{1}H NMR spectrum (500 MHz, CD_3CN) of **1_B^{2-}@Co$_3$TriCage** recorded at 25 °C. (B) Truncated ^{1}H NMR spectrum (500 MHz, CD_3CN) of **(1_A^-)(1_B^{2-})@Co$_3$TriCage** recorded at 70 °C. Labels of signals correspond to those in Schemes 2 and 3.

benzoate anions coordinate to the cobalt sites of **Co$_3$TriCage**,[11e] suggesting **1_B^{2-}** engages in similar interactions inside this host. The approximately equal sizes of the groups of β CH signals indicate that the carboxylate end of **1_B^{2-}** coordinates to two of the cobalt centers in the host, either simultaneously via a bridging interaction or by fast exchange between the two cobalt ions.

Resonances of the pyridyl groups and tmeda ligands of **Co$_3$TriCage** are also split to varying extents upon binding **1_B^{2-}**. The tmeda region of the spectrum, in particular, shows several signals, two of which are shifted downfield by > 1 ppm from those of the empty host. The considerable desymmetrization of the spectrum of **1_B^{2-}@Co$_3$TriCage** suggests that **1_B^{2-}** cannot reposition itself freely in this host (aside from possible exchange of the carboxylate group between two Co^{II} sites). These findings are consistent with rigid binding enforced by an $ArCO_2^-$→Co^{II} interaction. However, the host does not appear to support more than one such interaction despite possessing three Co^{II} sites. Thus, adding a second equivalent of **1_B^{2-}** to **1_B^{2-}@Co$_3$TriCage** results in partial precipitation of the complex from solution and broadening of its NMR signals without changing their chemical shifts (Figure S23). These observations suggest against strong association of the second **1_B^{2-}** guest, presumably because electrostatic repulsion prevents two CO_2^- groups from binding near the center of the cage. Consistent with weak binding of the second **1_B^{2-}** guest, we were unable to observe a 1:2 complex by ESI(+)-HRMS.

Guest **1_B^{2-}** also shows negative cooperativity for association in **Zn$_3$TriCage**, but the higher Lewis acidity[11e,16] of Zn^{II} reinforces binding of this guest enough to enable clear identification of both a 1:1 and 1:2 complex by ^{1}H NMR spectroscopy (Figures S48 and S50) and ESI(+)-HRMS (Figures S59 and S60). The 1:1 complex is formed quantitatively upon adding 1 equiv of **1_B^{2-}** to **Zn$_3$TriCage**, producing an NMR spectrum (Figure S48) in which most of the aromatic resonances of the cage are split into two distinct signals of equal size, suggesting loss of mirror symmetry between the two triangular faces. Most of the aromatic signals are well defined, but the 2-position CH resonance of the pyridyl groups is broadened and only one such signal is seen, corresponding to just half of these CH positions. Heating the sample to 60 °C led to the appearance of the missing 2-position signal and considerable sharpening of the other signals of the host (Figure S49), yielding a spectrum that clearly corresponds to a structure with time-averaged C_3 symmetry. Conversely,

https://doi.org/10.26434/chemrxiv-2024-4w50c-v2 **ORCID:** https://orcid.org/0000-0003-0035-4565 Content not peer-reviewed by ChemRxiv. **License:** CC BY-NC-ND 4.0

cooling to −40 °C produced an NMR spectrum consistent with a low symmetry structure (Figure S49).

A detailed analysis is impractical for the many broad and overlapping signals in the low-temperature spectrum of **1_B^{2-}@Zn_3TriCage**, but insights were gained by comparison with the spectrum acquired at 25 °C for the 1:2 complex **$(1_B^{2-})_2$@Zn_3TriCage** (Figures S50, S51). The latter spectrum is also complicated, but nearly every aromatic peak is sharp, allowing confident assignment of C_2 symmetry based on minimum integrals of 2H for signals in this region. This symmetry implies that two of the Zn^{II} sites are equivalent, and thus, both guests must coordinate to zinc centers. Notably, distinct signals near 7.25 and 9.75 ppm in the spectrum of the 1:2 complex match similar resonances in the low temperature spectrum of the 1:1 complex (Figure S51). Likewise, both spectra display broad resonances for the guest between 6 – 6.5 ppm, suggesting **1_B^{2-}** has a similar binding mode in both the 1:1 and 1:2 complexes.

Interactions of **1_B^{2-}** with **TriCage** differ significantly from those of this guest with the metallated hosts. The ^{1}H NMR spectrum of **TriCage** is only slightly altered after adding 0.5 equiv of **1_B^{2-}** (Figure S37), but further additions broaden and shift the signals of the host until ≥1.5 equiv **1_B^{2-}** have been added, at which point some resonance partially resharpen. These observations suggest that two **1_B^{2-}** guests bind cooperatively in **TriCage** and that the resulting complex engages in fast exchange with the empty host on the NMR timescale. However, definitive interpretation of the mode of binding is hindered because many signals remain broad after 2 equiv **1_B^{2-}** have been added, at which point the complex begins to precipitate. Furthermore, small additional signals are observed that presumably correspond to other modes of interaction between **1_B^{2-}** and **TriCage** (Figure S35, S36), but the nature of these interactions could not be determined. Despite these limitations, it can be concluded that **1_B^{2-}** associates with **TriCage** and that these interactions differ from those with the metallated hosts. A 1:2 binding stoichiometry appears likely but is not certain since only a 1:1 complex **1_B^{2-}@TriCage** was observable by ESI(+)-HRMS (Figure S55).

Host-guest complexes containing one equivalent each of **1_A^-** and **1_B^{2-}** (1:1:1 complexes, Scheme 3) were also characterized. The complex **$(1_A^-)(1_B^{2-})$@Co_3TriCage** has a ^{1}H NMR spectrum resembling that of **$(1_A^-)_2$@Co_3TriCage** except that the β CH signals are so broadened for the 1:1:1 complex as to barely be identifiable (Figure S16). Heating to 70 °C led to the resolution of these signals into two broad resonances centered near 14.97 and 16.83 ppm (Figure 2B).

Scheme 3. Complexes of the mixed-protonation-state guests 1_A^- and 1_B^{2-} in M_3TriCage (M = Co, Zn, H_2).

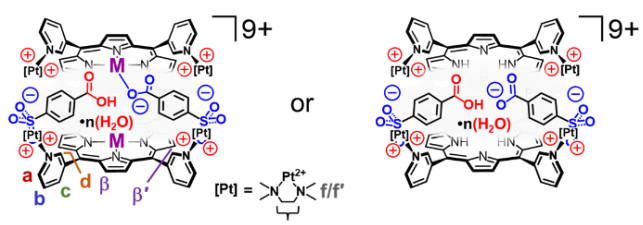

These downfield chemical shifts suggest that **1_B^{2-}** coordinates to cobalt, and the observation of just two β CH signals indicates that the carboxylate group exchanges rapidly among the three Co^{II} sites at 70 °C. Other regions of the spectrum also indicate high symmetry (D_{3h}), suggesting that the two guests readily exchange between which is protonated and which is coordinated to cobalt. In addition to NMR characterization, **$(1_A^-)(1_B^{2-})$@Co_3TriCage** was also observed by ESI(+)-HRMS (Figure S57).

Formation of **$(1_A^-)(1_B^{2-})$@Zn_3TriCage** was investigated by adding an equivalent of **1_A^-** to **1_B^{2-}@Zn_3TriCage**, producing a ^{1}H NMR spectrum reminiscent of those of the other complexes, but with multiple overlapping features observed for the signals of the host (Figure S46). Additionally, no resonance can be discerned for the pyridyl 2-position CH bonds that face the interior of the cage. The missing and poorly defined signals suggest that multiple conformations of the 1:1:1 complex form and exchange slowly on the NMR timescale. The signals of the complex are much better defined at 70 °C (Figure S47), but the spectrum remains complex, suggesting that rearrangements of the two guests still do not occur quickly on the NMR timescale. Strong coordination of **1_B^{2-}** to zinc is likely responsible for the slower dynamics of this complex relative to its Co^{II} counterpart.

Lastly, unmetallated **TriCage** binds **1_A^-** and **1_B^{2-}** to reveal an NMR spectrum (Figure S32) with features resembling those of its 1:2 complex with **1_A^-**, except for two signals that are broadened or missing: no signal is seen for the inward-facing pyridyl CH bonds, and significant broadening occurs for the resonance(s) of the porphyrin β CH positions facing the apertures of the cage. This latter signal is somewhat better resolved at 70 °C (Figure S33), yielding a spectrum that would be consistent with D_{3h} symmetry if not for the missing pyridyl CH resonance. Since the chemical shift of these pyridyl CH bonds is highly influenced by guests, and the separation between two NMR resonances affects their coalescence,[17] it is plausible that the sulfonate groups exchange too slowly between binding sites to average these CH signals, while the rest of the spectrum corresponds to higher symmetry. It is conceivable that repositioning of guests in **$(1_A^-)(1_B^{2-})$@TriCage** is slowed by CO_2^----HO_2C interactions that prevent the guests from moving independently.

The host-guest complexes described above provide useful subjects for studying confinement effects on acidity. Thus, it is useful to highlight key observations regarding these complexes: (1) All three cages bind **1_A^-** with positive cooperativity to yield 1:2 host-guest complexes. The CO_2H resonance could not be identified for these complexes, but upfield shifts of the CH signals of the guests (Figures S39-S43) suggest the guests sit deep inside each host.[18] (2) Guest **1_B^{2-}** binds with negative cooperativity in the Co_3 and Zn_3 cages, forming 1:1 complexes in which the CO_2^- group coordinates to a metal site. This interaction is also seen for a second **1_B^{2-}** guest binding in the Zn_3 host, while the Co_3 derivative supports only one such interaction. Association of **1_B^{2-}** with **TriCage** shows that metal sites are not essential for binding this guest. (3) All three cages form 1:1:1 complexes with the guests in their mixed protonation states **1_A^-** and **1_B^{2-}**. Carboxylate-metal coordination is seen for these complexes in the metallated hosts, while hydrogen bonding between the guests likely occurs in **$(1_A^-)(1_B^{2-})$@TriCage**.

https://doi.org/10.26434/chemrxiv-2024-4w50c-v2 **ORCID:** https://orcid.org/0000-0003-0035-4565 Content not peer-reviewed by ChemRxiv. **License:** CC BY-NC-ND 4.0

Hydration of the host-guest complexes. Solvation often has a profound influence on acid-base chemistry,[3b-e,6h,7b,19] so it is notable that water associates readily with most of the complexes described in the previous section. Association of water is evident from differences in the ^{1}H NMR spectra of **(1$_A^-$)$_2$@M$_3$TriCage** (M = Co, Zn, H$_2$) acquired in anhydrous CD_3CN vs. solvent that has absorbed ambient moisture (the latter being the conditions used in the previous section). For example, differences are seen in the signals of the tmeda ligands of **(1$_A^-$)$_2$@Co$_3$TriCage** in wet vs. dry conditions (Figure 3A), whereas the spectrum of empty **Co$_3$TriCage** is unaffected. Titration of an anhydrous solution of **(1$_A^-$)$_2$@Co$_3$TriCage** (1 mM) with water resulted in conversion between the dry and hydrated presentations of the ^{1}H NMR spectrum by the time 10 equiv H_2O (10 mM) had been added (Figure S15), suggesting fairly strong interaction of water with the complex.

Complexes of **1$_A^-$** with **TriCage** and **Zn$_3$TriCage** also showed the influence of water on host-guest interactions. Several signals of **(1$_A^-$)$_2$@TriCage** were shifted and/or broadened in the absence of water, especially the porphyrin NH resonance and signals of the host arising from aromatic CH bonds nearest to its apertures (Figures S29, S30). Furthermore, signals consistent with formation of a 1:1 complex were observed to appear and disappear up titration of **1$_A^-$** into an anhydrous solution of **TriCage** (Figure S31). Similar observations were made for interactions of **1$_A^-$** with anhydrous samples of **Zn$_3$TriCage** (Figures S44 and S45), and thus, it appears that hydration of the pore is needed to promote cooperative association of **1$_A^-$** in the TriCages. This is an interesting finding since aqueous solvation ordinarily weakens the dimerization of carboxylic acids. Apparently, the constraints of the nanocavity make it more favorable for the CO_2H groups to hydrogen bond with water rather than directly with each other. In comparison, the *p*-tolylSO_3^- guests in **(2$^-$)$_2$@TriCage**[11d] were found to induce much weaker interactions with water.

The ^{1}H NMR spectrum of **1$_B^{2-}$@Co$_3$TriCage** also differs significantly between anhydrous and wet conditions. The most downfield β CH signal is shifted by approximately +2 ppm in the absence of water (Figure 3B), and likewise, the most downfield signal of the tmeda ligand is found over 0.5 ppm more downfield under anhydrous conditions. Nearly full conversion between the dry and hydrated states was achieved upon titration with 40 equiv H_2O (40 mM, Figure S26), revealing that the confined environment in this complex hydrates less readily than the protonated state.

This observation is notable since water, being a highly polar solvent, usually stabilizes the ionic state of an acid-base pair,[19c] but in the confines of **Co$_3$TriCage**, water appears to interact less strongly with the deprotonated carboxylate guest **1$_B^{2-}$** than with its conjugate acid. The effects of water on interactions between **1$_B^{2-}$** and **TriCage** were also tested, finding that complexation is weaker under anhydrous conditions,[20] leading to greater precipitation of the host when **1$_B^{2-}$** was added (Figure S38). Lastly, the ^{1}H NMR signal of water is broadened and shifted upfield by the 1:1 complex between **Zn$_3$TriCage** and **1$_B^{2-}$** but not by the 1:2 complex or empty host (Figure S52), suggesting that only the 1:1 complex is easily hydrated.

Interestingly, moisture barely affects the ^{1}H NMR spectrum of **(1$_A^-$)(1$_B^{2-}$)@Co$_3$TriCage** at 25 °C, though slight differences in chemical shifts are seen for the β CH signals under wet vs. dry conditions at 70 °C, suggesting some degree of hydration of the complex (Figure S21). Because changes to the spectrum are so subtle at 25 °C, it was difficult to directly evaluate how readily hydration occurs. However, as described in the next section, acid-base titration experiments revealed that water affects host-guest speciation in a way that indicates hydration is weaker for the 1:1:1 complex than for **1$_B^{2-}$@Co$_3$TriCage** and **(1$_A^-$)$_2$@Co$_3$TriCage**. Hydrogen-bond donation from the protonated guest to its conjugate base[19b,21] may be responsible for weakening interactions of the guests with water in the 1:1:1 complex. Interestingly, the different interactions of these complexes with water yield unexpected ways that hydration affects the acidities of the guests (see below), but since the strength of these effects is ultimately rather small ($\Delta pK_a \leq 0.5$), a more detailed analysis of interactions of water with the host-guest complexes was not pursued.

Acidity of encapsulated carboxylic acids. Titration experiments were performed to measure the acidities of the 1:2 complexes of **1$_A^-$** with the different TriCage derivatives in MeCN (Scheme 4). Each complex was titrated with a neutral *N*-donor base[19a] that was approximately matched in strength to the acidity of the host-guest complex, allowing the determination of the pK_a of the encapsulated guests (Table 1, Figures S61-S70) based on the known acidities of the protonated titrants. Because hydrated conditions are more relevant to possible electrocatalytic applications,[12,13] these studies were performed in solvent containing traces of water sufficient to fully hydrate the host-guest complexes. Note that traces of water might stabilize the conjugate acids

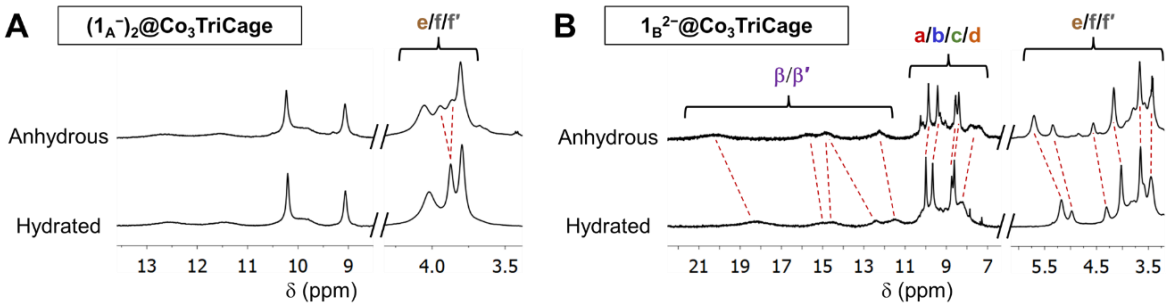

Figure 3. ^{1}H NMR spectra (500 MHz, CD_3CN, 25 °C) of the hydrated vs. anhydrous states of (A) **(1$_A^-$)$_2$@Co$_3$TriCage** showing changes to its tmeda resonances; and (B) **1$_B^{2-}$@Co$_3$TriCage** showing changes to nearly all signals of the complex.

https://doi.org/10.26434/chemrxiv-2024-4w50c-v2 **ORCID:** https://orcid.org/0000-0003-0035-4565 Content not peer-reviewed by ChemRxiv. **License:** CC BY-NC-ND 4.0

Scheme 4. Deprotonations of $(1_A^-)_2$@M_3TriCage.

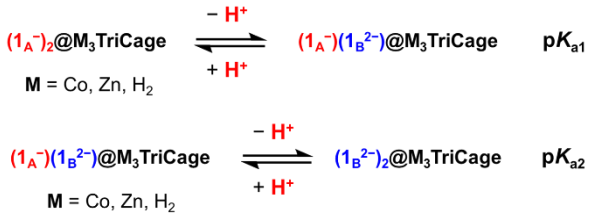

Table 1. Acidities host-guest complexes of 1_A^-.

Acid	pK_{a1} in MeCN[a] (in dry MeCN)	pK_{a2} in MeCN[a]
$\mathbf{1_A^-}$	20.75 ± 0.04[b]	N/A
$\mathbf{(1_A^-)_2}$**@Co$_3$TriCage**	16.53 ± 0.06[c] (~16.2)[d]	19.21 ± 0.04[e]
$\mathbf{1_A^-}$**@Co$_3$TriCage**	≤ 16.0 ± 0.15[f] (≥ 16.5)[g]	N/A
$\mathbf{1_A^-}$**@Co$^{II}_3$TriCage**	(≥ 24.5)[h]	N/A
$\mathbf{(1_A^-)_2}$**@TriCage**	18.2 ± 0.1[e]	20.4 ± 0.1[b]
$\mathbf{(1_A^-)_2}$**@Zn$_3$TriCage**	12.75 ± 0.07[i]	~14.5[j]

(a) Except where noted, pK_a values are the mean ± est. std. error of three acid-base titrations performed in CD_3CN containing ambient moisture (typically 50 – 100 mM water). (b) Measured with *N,N,N′,N′*-tetramethyl-1,3-butanediamine. (c) Measured with Et_2BnN. (d) From two titrations with Et_2BnN in dry CD_3CN. (e) Measured with Et_3N. (f) Estimated from the equilibrium $\mathbf{(1_A^-)_2}$**@Co$_3$Tri-Cage** + **Co$_3$TriCage** + 2 R_3N ⇄ 2 $\mathbf{1_B^{2-}}$**@Co$_3$TriCage** + 2 R_3NH^+. (g) Estimated using pK_{a1} of the diprotic complex under anhydrous conditions as the lower bound of K_{eff} for the equilibrium in caption f. (h) From cyclic voltammetry measured on the complex $\mathbf{1_B^{2-}}$**@Co$_3$TriCage**. (i) Measured with 2,6-lutidine, and (j) 2,4,6-collidine.

of the titrants by small amounts,[19a,c] potentially affecting the equilibria for deprotonating the encapsulated guests. However, this effect is of minor significance for comparing the host-guest complexes since large differences in pK_a were found between the complexes, these measurements showed good reproducibility, and water should have similar effects on all the bases employed.[19c]

Titration of $\mathbf{(1_A^-)_2}$**@Co$_3$TriCage** with Et_2BnN resulted in nearly complete conversion of the diprotic complex to its monoprotic state $\mathbf{(1_A^-)(1_B^{2-})}$**@Co$_3$TriCage** after 4 equiv of the amine had been added (Figure S63). These measurements revealed a pK_{a1} of 16.53 ± 0.06 for the diprotic complex, representing more than a 10,000-fold increase in acidity relative to that measured for the TBA^+ salt of $\mathbf{1_A^-}$ in MeCN (pK_a = 20.75 ± 0.04).[22,23] The increased acidity of the encapsulated guest can be attributed to stabilization of its conjugate base $\mathbf{1_B^{2-}}$ by the positive charge of the host, by hydrogen-bonding with the remaining protonated guest, and/or by coordination of CO_2^- to cobalt.[11e] This latter interaction is estimated to stabilize $\mathbf{1_B^{2-}}$ by at least 2.25 kcal mol^{-1} since the unmetallated complex $\mathbf{(1_A^-)_2}$**@TriCage** was less acidic by 1.7 pK_a units (pK_{a1} = 18.2 ± 0.1). Conversely, a much higher acidity was measured for the first deprotonation of $\mathbf{(1_A^-)_2}$**@Zn$_3$TriCage** (pK_{a1} = 12.75 ± 0.07), reflecting the greater Lewis acidity of Zn^{II} versus Co^{II}.[11e]

In all three hosts, the second $\mathbf{1_A^-}$ guest was more difficult to deprotonate than the first, though only by moderate amounts, with the smallest change in acidity measured for $\mathbf{(1_A^-)(1_B^{2-})}$**@Zn$_3$TriCage** (p$K_{a2}$ ≈ 14.5, Δp$K_{a1,2}$ ≈ 1.75). The high acidity maintained in this monoprotic complex indicates that, upon deprotonation, both guests coordinate to the zinc sites in $\mathbf{(1_B^{2-})_2}$**@Zn$_3$TriCage**. This necessarily places both CO_2^- groups near the center of the cage, so it is interesting that acidity is not decreased more by the electrostatic repulsion[4] of these groups. Apparently, the Zn^{II} sites are electron withdrawing enough to prevent anion-anion repulsion and CO_2H---^-O_2C hydrogen bonding from having very large effects on the acidity of the monoprotic state. In contrast, $\mathbf{(1_A^-)(1_B^{2-})}$**@Co$_3$TriCage** has a p$K_{a2}$ (19.21 ± 0.04) that is raised by a larger amount relative to the diprotic state (Δp$K_{a1,2}$ = 2.67), consistent with the inability of the second $\mathbf{1_B^{2-}}$ guest to coordinate to cobalt (see above).

The unmetallated complex $\mathbf{(1_A^-)(1_B^{2-})}$**@TriCage** also has an acidity (pK_a = 20.4 ± 0.1) that is more than two orders of magnitude lower than that of its diprotic state (Δp$K_{a1,2}$ = 2.2). This decrease can be attributed to $\mathbf{1_B^{2-}}$---$\mathbf{1_A^-}$ interactions that stabilize the monoprotic state of the complex and which should be maximized in the absence of metal sites for $\mathbf{1_B^{2-}}$ to coordinate to. Indeed, the lower acidity of $\mathbf{(1_A^-)(1_B^{2-})}$**@TriCage** relative to $\mathbf{(1_A^-)(1_B^{2-})}$**@Co$_3$TriCage** can be attributed to stronger guest-guest interactions in the former. Note, however, that these analyses ultimately suggest that interactions between $\mathbf{1_B^{2-}}$ and $\mathbf{1_A^-}$ are weak even in the unmetallated complex, representing a stabilization of only ~1.5 kcal mol^{-1} if it is assumed that the guest-guest interactions increase the acidity of the diprotic state by as much as the acidity of the monoprotic state is decreased. Even if this assumption does not hold, it can still be concluded that $\mathbf{1_B^{2-}}$---$\mathbf{1_A^-}$ interactions are weaker than $\mathbf{1_B^{2-}}$→Co^{II} coordination, hence the lower acidities for the complexes of the unmetallated host.

Additional experiments were performed to probe how guest-guest interactions affect the acidity of the 1:2 complex $\mathbf{(1_A^-)_2}$**@Co$_3$TriCage**. An equimolar mixture of this complex and empty **Co$_3$TriCage** was titrated with Et_3N, resulting in the formation of the 1:1 complex $\mathbf{1_B^{2-}}$**@Co$_3$TriCage** (Eq 1)

$$\mathbf{(1_A^-)_2}\text{@Co}_3\text{TriCage} + \text{Co}_3\text{TriCage} + 2\ \text{Et}_3\text{N} \rightleftharpoons 2\ \mathbf{1_B^{2-}}\text{@Co}_3\text{TriCage} + 2\ \text{Et}_3\text{NH}^+ \quad (1)$$

with little of the 1:1:1 complex $\mathbf{(1_A^-)(1_B^{2-})}$**@Co$_3$TriCage** detected by ^{1}H NMR spectroscopy during the experiment (Figure S65). This observation implies that cooperative binding of the two guests in $\mathbf{(1_A^-)_2}$**@Co$_3$TriCage** must be more favorable than in $\mathbf{(1_A^-)(1_B^{2-})}$**@Co$_3$TriCage.** The deprotonation of the 1:2 complex in the presence of empty host was fitted to a simple acid-base equilibrium to give an effective

https://doi.org/10.26434/chemrxiv-2024-4w50c-v2 **ORCID:** https://orcid.org/0000-0003-0035-4565 Content not peer-reviewed by ChemRxiv. **License:** CC BY-NC-ND 4.0

p$K_{a(Eff)}$ of 16.8 ± 0.15, and this value was deconvoluted into contributions from formation of the 1:1 complex **1_A^-@Co$_3$TriCage** followed by the equilibrium for deprotonating this complex (Figure S65). A K of ≤ 0 .0075 can be estimated for the first of these equilibria based on HRMS data for a 1:1 mixture of **1_A^-** and **TriCage** (Figure S54), implying a pK_a ≤ 16.0 ± 0.15 for deprotonation of **1_A^-@Co$_3$TriCage**. Thus, even based on the upper bound of this pK_a estimate, the 1:1 complex of **1_A^-** in **Co$_3$TriCage** appears to be more acidic than the corresponding 1:2 complex.[24]

Lastly, titrations of **(1_A^-)$_2$@Co$_3$TriCage** with Et_2BnN were performed under anhydrous conditions, revealing a pK_a (~16.2) that is just slightly lower than that measured in the hydrated complexes.[25] Interestingly, titration of Et_2BnN into an equimolar mixture of **1_A^-** and **Co$_3$TriCage** in dry CD_3CN produced **(1_A^-)(1_B^{2-})@Co$_3$TriCage** as the only deprotonated complex formed, reversing the behavior seen in wet solvent. This finding indicates that water must stabilize **(1_A^-)$_2$@Co$_3$TriCage** and **1_B^{2-}@Co$_3$TriCage** relative to **(1_A^-)(1_B^{2-})@Co$_3$TriCage**, implying that the 1:1:1 complex has the weakest interactions with water.

Taken together, the above findings reveal subtle counterintuitive effects of hydration and guest-guest interactions on the acidity of **1_A^-** bound in **Co$_3$TriCage**. In particular, the 1:2 complex **(1_A^-)$_2$@Co$_3$TriCage** is stabilized by cooperative interactions between water and the two **1_A^-** guests, producing a somewhat lower acidity than that of the 1:1 complex **1_A^-@Co$_3$TriCage** under comparable conditions. Water and CO_2H---^-O_2C interactions both can increase the acidities of carboxylic acids in bulk MeCN,[19,21] so it is interesting that hydration and guest-guest interactions combine to produce the opposite effect in **(1_A^-)$_2$@Co$_3$TriCage**. In the absence of water, however, the estimated acidity of the 1:1 complex (pK_a ≥ 16.5) is lower than that of the 1:2 complex, consistent with the favorable **1_B^{2-}---1_A^-** interactions expected upon deprotonation of the latter.[21]

Effects of pore reduction on acidity. Cyclic voltammetry was used to measure the Co^{II}/Co^{I} reduction potentials of the complexes of **1_A^-** and **1_B^{2-}** in **Co$_3$TriCage**, allowing the acidities of the reduced states of these complexes to be calculated.[26] The 1:2 complex of **1_A^-** shows a single broadened 3 e$^-$ $Co^{II/I}$ redox couple centered at −1.03 V vs $Fc^{+/0}$ (Figure 4A), which is just 50 mV negative of the corresponding reduction of **Co$_3$TriCage**.[11c] The deprotonated 1:1 complex **1_B^{2-}@Co$_3$TriCage** exhibits a similar reversible reduction ($E_{1/2}$ = −1.00 V) but also a smaller quasireversible redox couple at $E_{1/2}$ = −1.47 V (Figure 4B). The more positive feature is assigned to the Co^{II}/Co^{I} reduction of the two free Co^{II} centers while the more negative feature corresponds to the Co^{II} site that coordinates **1_B^{2-}** (Scheme 5). The 470 mV cathodic shift of this reduction indicates that the $ArCO_2^-$ group is destabilized by 11 kcal mol^{-1}, which is too large to correspond to just the strength of the CO_2^-→Co^{II} interaction (~4 kcal mol^{-1}).[27] Thus, the extra ~7 kcal mol^{-1} destabilization can be attributed to the unfavorable electrostatic interactions between the carboxylate group and the three anionic Co^{I} sites in the reduced zwitterionic state of the host.

The destabilization of **1_B^{2-}** in **1_B^{2-}@Co$^{I}_3$TriCage** corresponds to an increase in the pK_a of **1_A^-@Co$^{I}_3$TriCage** by 8 units relative to that of its *tris*-Co^{II} state under anhydrous conditions. Thus, a pK_a of ≥ 24.5 can be determined for **1_A^-** when bound in the reduced host, providing an unprecedented measurement of how charging a porous structure with electrons affects the thermodynamics of proton transfer in its interior,[26] representing a key consideration for electrocatalysis in nanoconfined environments.[14] The complex **(1_A^-)(1_B^{2-})@Co$_3$TriCage** also shows an extra cathodic feature that suggests the acidity of **(1_A^-)$_2$@Co$_3$TriCage** is decreased considerably by reduction (Figure 4C). However, the change in acidity cannot reliably be estimated since the reduction feature is irreversible and changes in its exact appearance and position over multiple cycles.

Control experiments examined the CVs of 1:2 complexes between **Co$_3$TriCage** and either *p*-tolylSO_3^- (**2**$^-$) or 4-sulfanatomethylbenzoate (**3**$^-$). Both complexes show a single reversible reduction near −1 V vs. $Fc^{+/0}$ (Figures S71, S72), confirming that the extra redox features near −1.5 V for

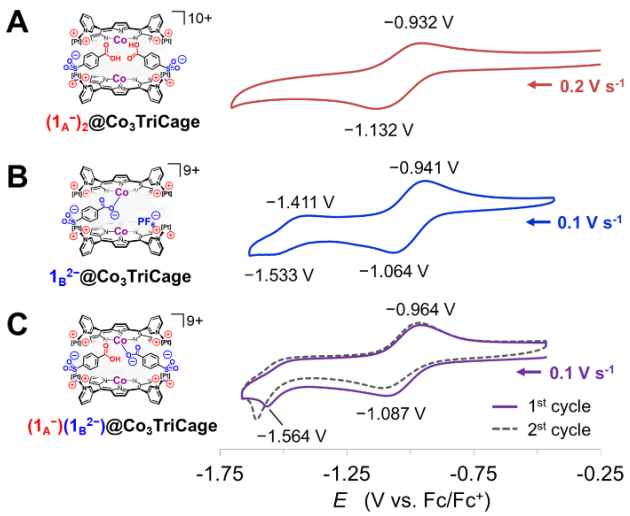

Figure 4. Cyclic voltammograms of (A) **(1_A^-)$_2$@Co$_3$TriCage**, (B) **1_B^{2-}@Co$_3$TriCage**, and (C) **(1_A^-)(1_B^{2-})@Co$_3$TriCage** recorded using a GCWE in MeCN containing 0.1 M $TBAPF_6$.

Scheme 5. Reduction of the 1:1 complex 1_B^{2-}@Co$_3$TriCage as observed by cyclic voltammetry and NMR spectroscopy.

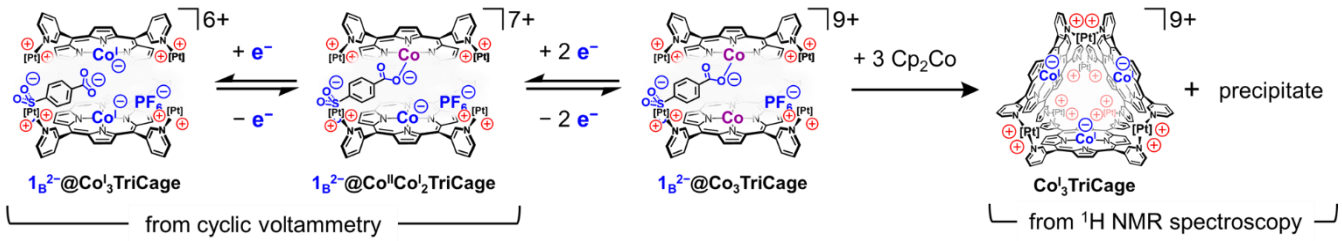

https://doi.org/10.26434/chemrxiv-2024-4w50c-v2 **ORCID:** https://orcid.org/0000-0003-0035-4565 Content not peer-reviewed by ChemRxiv. **License:** CC BY-NC-ND 4.0

complexes of $\mathbf{1_B}^{2-}$ can be attributed to $CO_2^- \rightarrow Co^{II}$ coordination. Likewise, titration of [TBA][OAc] into a 1 mM sample of [(*N*-methyl-3-pyridinium)$_4$porphyrinCo^{II}]$^{4+}$ produced a gradual cathodic shift of the $Co^{II/I}$ redox couple, reaching a $\Delta E_{1/2}$ of −115 mV at a 50 mM concentration of acetate (Figure S73). This finding confirms that metal-carboxylate coordination alters the redox features of Co^{II} sites, while also revealing that this effect is much weaker outside the nano-confined environment of **Co$_3$TriCage**.

^{1}H NMR spectroscopy was used to attempt to observe the diamagnetic *tris*-Co^I states of the host-guest complexes, as accessed via reduction of the host with Cp_2Co in CD_3CN. Addition of $\mathbf{2}^-$ to **Co$^I_3$TriCage** leads to the appearance of NMR signals consistent with strong, non-cooperative 1:2 binding of this guest (Figure S74), similar to what we have reported for association of $\mathbf{2}^-$ with unmetallated **TriCage**.[11d] In contrast, reduction of $\mathbf{1_B}^{2-}$**@Co$^I_3$TriCage** with 3 equiv Cp_2Co leads to a ^{1}H NMR spectrum matching that of empty **Co$^I_3$TriCage**,[11c] with integration indicating significant precipitation of the host from solution (Figure S75). Thus, $\mathbf{1_B}^{2-}$ appears to be ejected from the reduced host (Scheme 5), leading to partial precipitation of the host as seen for the other TriCages in the presence of excess $\mathbf{1_B}^{2-}$. These findings are consistent with strong destabilization of the anionic CO_2^- group in the reduced state of the host.

Computational optimization of host-guest structures. It was not possible to obtain single-crystal X-ray diffraction data of sufficient quality to structurally characterize the complexes of $\mathbf{1_A}^-$ and/or $\mathbf{1_B}^{2-}$ in any of the TriCage derivatives, so computational analyses were employed to better understand how these guests sit inside the three hosts. Initial Hartree-Fock structural optimizations were followed by DFT optimizations (B3LYP functional;[28] 6–31++G** basis set for light atoms and LANL2DZ for metals[29]), revealing 2 – 3 possible geometries for each complex containing two of the functional guests in any combination of protonation states (Figures 5 and S77 – S79). In all cases, the lowest energy structures agreed well with experimental results, providing additional insight into the origins of the host-guest and acid-base properties of these complexes.

For each host, the lowest energy **($\mathbf{1_A}^-$)$_2$@M$_3$TriCage** structure has the SO_3^- groups of the two guests sitting along the edges of different porphyrin units (Figures 5A, S77E, S79E), whereas the experimentally determined structures of **TriCage** and related hosts tend to show two encapsulated anions sitting along opposite edges of the same porphyrin wall.[11a,d] Indeed, this latter anion placement was found upon optimizing complexes with one $\mathbf{1_A}^-$ and one PF_6^- guest (Figures 5B, S77A, S79A). It is likely that the less symmetric placement of the anions is favored in complexes with two $\mathbf{1_A}^-$ guest in order to accommodate the efficient packing of two lengthy benzoic acid units inside the hosts. In comparison, significantly higher energies (by 8 – 9 kcal mol^{-1}) were obtained for structures with a more symmetric placement of two $\mathbf{1_A}^-$ guests, even when this allows for hydrogen bonding between the guests (Figures S77C, S78C, S79C). Notably, since the guests do not hydrogen bond with each other in the lowest energy structures of **($\mathbf{1_A}^-$)$_2$@M$_3$TriCage**, the CO_2H groups of both guests are exposed inside the hydrophobic cavity, possibly explaining why these complexes can be hydrated so easily. However, since water has only a small effect on the acidity of these complexes, we did not try to model specific interactions with water.

The lowest energy structures of the 1:1:1 complexes **($\mathbf{1_A}^-$)($\mathbf{1_B}^{2-}$)@M$_3$TriCage** are also similar across the three hosts, though in these cases the SO_3^- groups sit at opposite ends of a single porphyrin unit in order to accommodate hydrogen bonding between the guests[19b,21] (Figures 5C, S77F, S79F). The resulting CO_2H---^-O_2C interactions are characterized by short O---O distances of 2.46 – 2.6 Å, representing strong hydrogen bonding[5a] across the series of 1:1:1 complexes even though the CO_2^- group also coordinates to metal sites in the cobalt and zinc derivatives. Interestingly, the CO_2^- group bridges between two metal sites in these derivatives, while the optimized structures of the 1:1 complexes $\mathbf{1_B}^{2-}$**@M$_3$TriCage** has just a single oxygen atom coordinated to cobalt or zinc (Figures 5D and S79B). This difference may be the result of π-π interactions between the host and the additional $\mathbf{1_A}^-$ guest in the 1:1:1 complexes, which would reinforce the contraction of the host that is needed to facilitate a second metal-oxygen interaction. Regardless of the cause,

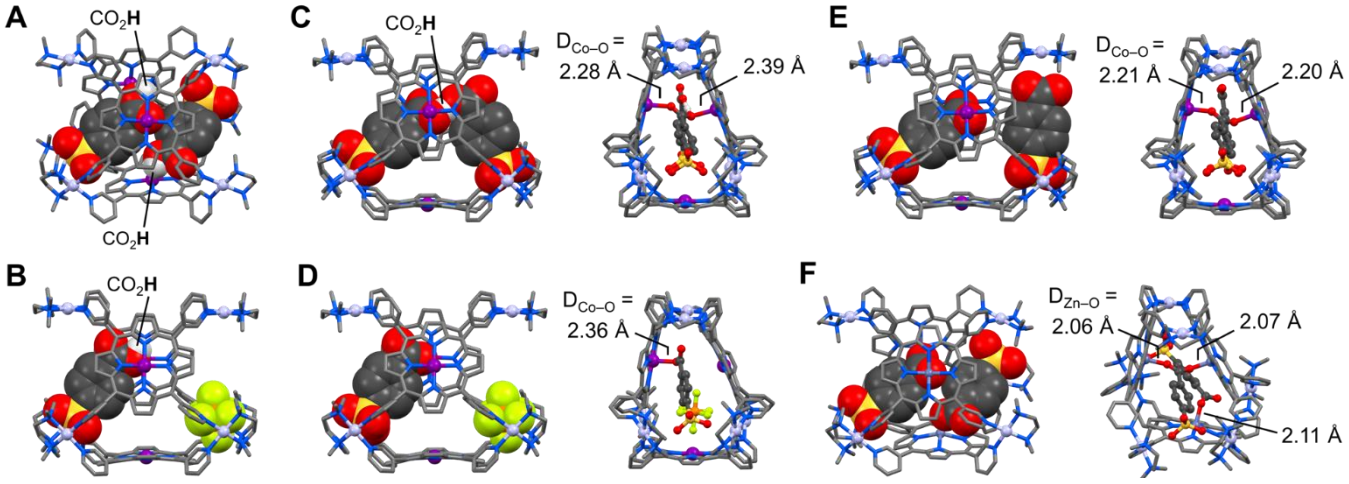

Figure 5. Lowest energy computationally (DFT) optimized structures of (A) **($\mathbf{1_A}^-$)$_2$@Co$_3$TriCage**, (B) **($\mathbf{1_A}^-$)(PF_6^-)@Co$_3$TriCage**, (C) **($\mathbf{1_A}^-$)($\mathbf{1_B}^{2-}$)@Co$_3$TriCage**, (D) **($\mathbf{1_B}^{2-}$)(PF_6^-)@Co$_3$TriCage**, (E) **($\mathbf{1_B}^{2-}$)$_2$@Co$_3$TriCage**, (F) **($\mathbf{1_B}^{2-}$)$_2$@Zn$_3$TriCage**.

https://doi.org/10.26434/chemrxiv-2024-4w50c-v2 **ORCID:** https://orcid.org/0000-0003-0035-4565 Content not peer-reviewed by ChemRxiv. **License:** CC BY-NC-ND 4.0

the narrowed cavity and multiple stabilizing interactions of the CO_2^- and CO_2H groups might explain why **(1_A^-)(1_B^{2-})@Co_3TriCage** has weaker interactions with water than the other complexes of these guests.

In contrast to the monoprotic and diprotic states, the fully deprotonated complexes **(1_B^{2-})$_2$@M_3TriCage** show different optimized structures for each host. In the cobalt version (Figure 5E), one of the $\mathbf{1_B^{2-}}$ guests maintains similar interactions with the host as seen in the 1:1:1 complex, including the bridging of the CO_2^- group between two Co^{II} sites. However, the second $\mathbf{1_B^{2-}}$ guest takes on a different binding mode in which its CO_2^- group is shifted away from the interior of the cage, interacting instead with one of the (tmeda)Pt^{2+} units at one of the apertures of the host. Notably, this binding mode is seen for both of the $\mathbf{1_B^{2-}}$ guests in the optimized structure of **(1_B^{2-})$_2$@TriCage** (Figure S77I), as expected based on the similar acidities of the 1:1:1 complexes in the unmetallated and cobalt-metallated hosts (see above). Lastly, **(1_B^{2-})$_2$@Zn_3TriCage** has both CO_2^- groups coordinated to Zn^{II} sites (Figure 5F) consistent with the high acidities measured for both **(1_A^-)$_2$@Zn_3TriCage** and **(1_A^-)(1_B^{2-})@Zn_3TriCage** (see above). It is notable that the Zn^{II} sites are sufficiently electron withdrawing to allow the anionic carboxylate groups to sit only about 5.3 Å from each other (measured between the carbon atoms), whereas an analogous structure for **(1_B^{2-})$_2$@Co_3TriCage** was found to be ~3.5 kcal mol^{-1} higher in energy than the geometry with only one CO_2^- group coordinated to Co^{II} (Figures S78I,K)

Summary and Conclusions.

In summary, we have found that three **M_3TriCage** derivatives (M = H_2, Co, Zn) can bind 4-sulfanatobenzoic acid ($\mathbf{1_A^-}$) and/or its conjugate base ($\mathbf{1_B^{2-}}$) to form host-guest complexes containing up to two of these guests in any combination of protonation states. These complexes alter the pK_a of $\mathbf{1_A^-}$ to a remarkable extent (pK_a = 12.75 to ≥ 24.5), with the acidity of this guest increased by 8 orders of magnitude in **(1_A^-)$_2$@Zn_3TriCage** and 4 orders of magnitude in **(1_A^-)$_2$@Co_3TriCage**, while its acidity is decreased 4 orders of magnitude in the reduced complex **1_A^-@Co^I_3TriCage**. In comparison, unmetallated **(1_A^-)$_2$@TriCage** increases the acidity of $\mathbf{1_A^-}$ by just 2.5 pK_a units despite contributions from Coulombic effects and other factors (e.g., hydrogen bonding, pore hydration) that might be expected to increase the acidity of the guest. Thus, the **M_3TriCages** are distinguished by the dominant effects of the metal sites on altering acid-base chemistry.

In the most obvious effect, Lewis acidic Zn^{II} and Co^{II} ions increase the Brønsted acidity of $\mathbf{1_A^-}$ by stabilizing its deprotonated state $\mathbf{1_B^{2-}}$. In a more subtle corollary, $CO_2^- \rightarrow Zn^{II}$ interactions withdraw enough electron density from $\mathbf{1_B^{2-}}$ to stabilize two CO_2^- groups in close proximity, leading to relatively small changes of acidity for sequential deprotonation of two encapsulated $\mathbf{1_A^-}$ guests. Conversely, the carboxylate group is destabilized by ~7 kcal mol^{-1} in the reduced complex **1_B^{2-}@Co^I_3TriCage** due to Coulombic interactions with the anionic Co^I sites. This observation implies a large increase in the basicity of the encapsulated CO_2^- group, which is, to our knowledge, the first measurement of how a pore lined with redox-active metal sites[11-13] can alter the thermodynamics of proton transfer. Similar behavior has been characterized in metalloproteins,[4a] so these results establish an interesting parallel between the redox chemistry of **Co_3TriCage** and certain proteins.

Beyond fundamental novelty, these findings shed light on how porous materials might affect electrocatalytic processes. For example, the turnover frequencies of a number of important reactions can be influenced by the relative acidities of catalytic intermediates, proton relays, and the terminal source of H^+,[14a,b] so it is valuable to understand how porous nanostructures can be used to tune these thermodynamic relationships. From a different perspective, the $ArCO_2^-$ guests are reminiscent of metal-bound CO_2^- intermediates that are often invoked in the reduction of CO_2.[30] Our findings suggest that Lewis acidic metalloporphyrins may be especially useful for dissipating the charge of these intermediates in nanoconfined active sites.

Lastly, it is worth commenting on the interactions of water with **Co_3TriCage** and its complexes with $\mathbf{1_A^-}$ and $\mathbf{1_B^{2-}}$. Hydration of the host-guest complexes has a surprisingly weak influence on the acid-base equilibrium between these guests,[3b-e] but it is still notable that both guests are readily hydrated inside the host, while empty **Co_3TriCage** has weak interactions with water even in its zwitterionic *tris*-Co^I state (Figure S76). Since water is important for proton transport in confined environments,[14c,31] these observations provide a mechanistic underpinning for the common observation[12a,13a,e,f] that hydrophobic porphyrin nanomaterials favor CO_2 reduction over H^+ reduction: if hydration of the active site is inhibited until a metal-bound CO_2^- intermediate forms, then H^+ will not be able to access the reduced metal sites. However, we caution that more investigation is needed to better understand how hydration influences the electrochemical properties of the **M_3TriCage**, especially with respect to the kinetics of H^+ transport. We are currently pursuing such studies.

ASSOCIATED CONTENT

Synthetic and experimental procedures; 1D and 2D NMR spectra (^{1}H, ^{13}C{^{1}H}, COSY, ^{13}C-^{1}H HSQC and HMBC); ESI(+)-MS spectra; cyclic voltammograms; details of DFT calculations; and details of acid-base titration analyses. This material is available free of charge via the Internet via chemrxiv.org.

AUTHOR INFORMATION

Corresponding Author

Mark C. Lipke, Email: ml1353@chem.rutgers.edu.
Richard C. Remsing, Email: rick.remsing@rutgers.edu.

Present Addresses

†Department of Chemistry, Barnard College, Altschul Hall, 3009 Broadway, New York, NY 10027.

Author Contributions

‡T.J.J. and K.G.D. contributed equally to this work. All authors have given approval to the final version of the manuscript.

https://doi.org/10.26434/chemrxiv-2024-4w50c-v2 **ORCID:** https://orcid.org/0000-0003-0035-4565 Content not peer-reviewed by ChemRxiv. **License:** CC BY-NC-ND 4.0

Notes

The authors declare no competing financial interests.

ACKNOWLEDGMENT

M.C.L acknowledges the National Science Foundation (CHE award # 2204045) for financial support of this research. The authors also acknowledge Rutgers, The State University of New Jersey, for financial support of this research, and the Office of Advanced Research Computing (OARC) at Rutgers, The State University of New Jersey, for providing access to the Amarel cluster and associated research computing resources. We thank Professor Mir Bowring of Reed College for making us aware of reference 23.

REFERENCES

(1) (a) Grommet, A. B.; Feller, M.; Klajn, R. Chemical Reactivity Under Nanoconfinement. *Nat. Nanotech.* **2020**, *15*, 256 – 271. doi.org/10.1038/s41565-020-0652-2. (b) Yoshizawa, M.; Klosterman, J. K.; Fujita, M. Functional Molecular Flasks: New Properties and Reactions within Discrete, Self-Assembled Hosts. *Angew. Chem., Int. Ed*. **2009**, *48*, 3418 – 3438. doi.org/10.1002/anie.200805340. (c) Brown, C. J.; Toste, F. D.; Bergman, R. G.; Raymond, K. N. Supramolecular Catalysis in Metal-Ligand Cluster Hosts. *Chem. Rev.* **2015**, *115*, 3012 – 3035. doi.org/10.1021/cr4001226. (d) Bairagya, M. D.; Bujol, R. J.; Elgrishi, N. Fighting Deactivation: Classical and Emerging Strategies for Efficient Stabilization of Molecular Electrocatalysts. *Chem. Eur. J.* **2019**, *26*, 3991 – 4000. doi.org/10.1002/chem.201904499.

(2) (a) Muñoz-Santiburcio, D.; Wittekindt, C.; Marx, D. Nanoconfinement Effects on Hydrated Excess Protons in Layered Materials. *Nat. Commun.* **2013**, *4*, 2349. doi.org/10.1038/ncomms3349. (b) Muñoz-Santiburcio, D.; Marx, D. Chemistry in Nanoconfined Water. *Chem. Sci*. **2017**, *8*, 3444 – 3452. doi.org/10.1039/C6SC04989C. (c) Remsing, R. C.; McKendry, I. G.; Strongin, D. R.; Klein, M. L.; Zdilla, M. J. Frustrated Solvation Structures Can Enhance Electron Transfer Rates. *J. Phys. Chem. Lett.* **2015**, *6*, 4804 – 4808. doi.org/10.1021/acs.jpclett.5b02277. (d) Bhullar, R. K.; Zdilla, M. J.; Klein, M. L.; Remsing, R. C.; Effect of Water Frustration on Water Oxidation Catalysis in the Nanoconfined Interlayers of Layered Manganese Oxides Birnessite and Buserite. *J. Mater. Chem. A* **2021**, *9*, 6924 – 6932. doi.org/10.1039/D0TA09635K. (e) Dhattarwal, H.S.; Remsing, R. C.; Kashyap, H. K.; Intercalation–Deintercalation of Water-in-Salt Electrolytes in Nanoscale Hydrophobic Confinement. *Nanoscale*, **2021**, *13*, 4195–4205. doi.org/10.1039/D0NR08163A. (f) Bañuelos, J. L.; Borguet, E.; Brown, G. E.; Cygan, R. T.; DeYoreo, J. J.; Dove, P. M.; Gaigeot, M. P.; Geiger, F. M.; Gibbs, J. M.; Grassian, V. H.; Ilgen, A. G.; Jun, Y.; Kabengi, N.; Katz, L. E.; Kubicki, J. D.; Lützenkirchen, J.; Putnis, C. V.; Remsing, R. C.; Rosso, K. M.; Rother, G. Oxide– and Silicate–Water Interfaces and Their Roles in Technology and the Environment. *Chem. Rev.* **2023**, *123*, 6413 – 6544. doi.org/10.1021/acs.chemrev.2c00130. (g) Ashbaugh, H. S.; Gibb, B. C.; Suating, P. Cavitand Complexes in Aqueous Solution: Collaborative Experimental and Computational Studies of the Wetting, Assembly, and Function of Nanoscopic Bowls in Water. *J. Phys. Chem. B* **2021**, *125*, 3253– 3268. doi.org/10.1021/acs.jpcb.0c11017.

(3) (a) Churg, A. K.; Warshel, A. Control of the Redox Potential of Cytochrome and Microscopic Dielectric Effects in Proteins. *Biochemistry* **1986**, *25*, 1675 – 1681. doi.org/10.1021/bi00355a035. (b) Urry, D. W.; Gowda, C.; Peng, S.; Parker, T. M.; Jing, N.; Harris, R. D. Nanometric Design of Extraordinary Hydrophobic-Induced pKa Shifts for Aspartic Acid: Relevance to Protein Mechanisms. *Biopolymers* **1994**, *34*, 889 – 896. doi.org/10.1002/bip.360340708. (c) Isom, D. G.; Cannon, B. R.; Casteñeda, C. A.; Robinson, A.; García-Moreno, E. B. High Tolerance for Ionizable Residues in the Hydrophobic Interior of Proteins. *Proc. Nat. Acad. Sci. USA* **2008**, *105*, 17784 – 17788. doi.org/10.1073/pnas.0805113105. (d) Isom, D. G.; Casteñeda, C. A.; Cannon, B. R.; García-Moreno, E. B. Large Shifts in pKa values of Lysin Residues Buried Inside a Protein. *Proc. Nat. Acad. Sci. USA* **2011**, *108*, 5260 – 5265. doi.org/10.1073/pnas.1010750108. (e) Dwyer, J. J.; Gittis, A. G.; Karp, D. A.; Lattman, E. E.; Spencer, D. S.; Stites, W. E.; García-Moreno, E. B. High Apparent Dielectric Constants in the Interior of a Protein Reflect Water Penetration. *Biophys. J.* **2000**, *79*, 1610 – 1620. doi.org/10.1016/S0006-3495(00)76411-3.

(4) (a) Varadarajan, R.; Zewert, T. E.; Gray, H. B.; Boxer, S. G. Effects of Buried Ionizable Amino Acids on the Reduction Potential of Recombinant Myoglobin. *Science* **1989**, *243*, 69 – 72. doi.org/10.1126/science.2563171. (b) Westheimer, F. H. Coincidences, Decarboxylation, and Electrostatic Effects. *Tetrahedron* **1995**, *51*, 3 – 20. doi.org/10.1016/0040-4020(94)00865-R. (c) Warshel, A.; Sharma, P. K.; Kato, M.; Xiang, Y.; Liu, H.; Olsson, M. H. M. Electrostatic Basis for Enzyme Catalysis. *Chem. Rev.* **2006**, *8*, 3210 – 3235. doi.org/10.1021/cr0503106. (d) Pinitglang, S.; Watts, A. B.; Patel, M.; Reid, J. D.; Noble, M. A.; Gul, S.; Bokth, A.; Naeem, A.; Patel, H.; Thomas, E. W.; Sreedharan, S. K.; Verma, C.; Brocklehurst, K. A Classical Enzyme Active Center Motif Lacks Catalytic Competence until Modulated Electrostatically. *Biochemistry* **1997**, *36*, 9968 – 9982. doi.org/10.1021/bi9705974.

(5) (a) Cleland, W. W.; Frey, P. A.; Gertl, J. A. The Low Barrier Hydrogen Bond in Enzymatic Catalysis. *J. Biol. Chem.* **1998**, *273*, 25529 – 25532. doi.org/10.1074/jbc.273.40.25529. (b) Ha, N.-C.; Kim, M.-S.; Lee, W.; Choi, K. Y.; Oh, B-H. Detection of Large pK_a Perturbations of an Inhibitor and a Catalytic Group at an Enzyme Active Site, a Mechanistic Basis for Catalytic Power of Many Enzymes. *J. Biol. Chem.* **2000**, *275*, 41100 – 41106. doi.org/10.1074/jbc.M007561200. (c) Thurlkill, R. L.; Grimsley, G. R.; Scholtz, J. M.; Pace, C. N. Hydrogen Bonding Markedly Reduces the *p*K of Bured Carboxyl Groups in Proteins. *J. Mol. Biol.* **2006**, *362*, 594 – 604. doi.org/10.1016/j.jmb.2006.07.056.

(6) (a) Pluth, M. D.; Bergman, R. G.; Raymond, K. N. Making Amines Strong Bases: Thermodynamic Stabilization of Protonated Guests in a Highly-Charged Supramolecular Host. *J. Am. Chem. Soc.* **2007**, *129*, 11459 – 11467. doi.org/10.1021/ja072654e. (b) Pluth, M. D.; Bergman, R. G.; Raymond, K. N. Acid Catalysis in Basic Solution: A Supramolecular Host Promotes Orthoformate Hydrolysis. *Science* **2007**, *316*, 85 – 88. doi.org/10.1126/science.1138748. (c) Hong, C. M.; Morimoto, M.; Kapustin, E. A.; Alzakhem, N.; Bergman, R. G.; Raymond, K. N.; Toste, F. D. Deconvoluting the Role of Charge in a Supramolecular Catalyst. *J. Am. Chem. Soc.* **2018**, *140*, 6591–6595. doi.org/10.1021/jacs.8b01701. (d) Murase, T.; Nishijima, Y.; Fujita, M. Cage-Catalyzed Knoevenagel Condensation under Neutral Conditions in Water. *J. Am. Chem. Soc.* **2012**, *134*, 162– 164. doi.org/10.1021/ja210068f. (e) Cullen, W.; Misuraca, M. C.; Hunter, C. A.; Williams, N. H.; Ward, M. D. Highly Efficient Catalysis of the Kemp Elimination in the Cavity of a Cubic Coordination Cage. *Nat. Chem.* **2016**, *8*, 231 – 236. doi.org/10.1038/nchem.2452. (f) Cullen, W.; Metherell, A. J.; Wragg, A. B.; Taylor, C. G. P.; Williams, N. H.; Ward, M. D. Catalysis in a Cationic Coordination Cage Using a Cavity-Bound Guest and Surface-Bound Anions: Inhibition, Activation, and Autocatalysis. *J. Am. Chem. Soc.* **2018**, *140*, 2821 – 2828. doi.org/10.1021/jacs.7b11334. (g) Ngai, C.; Wu, H.-T.; da Camara, B.; Williams, C. G.; Mueller, L. J.; Julian, R. R.; Hooley, R. J. Moderated Basicity of Endohedral Amine Groups in an Octa-Cationic Self-Assembled Cage. *Angew. Chem., Int. Ed.* **2022**, *61*, e202117011. doi.org/10.1002/anie.202117011. (h) Cullen, W.; Thomas, K. A.; Hunter, C. A.; Ward, M. D. pH-Controlled Selection Between One of Three Guests from a Mixture Using a Coordination Cage Host. *Chem. Sci*. **2015**, *6*, 4025 – 4028. doi.org/10.1039/C5SC01475A.

(7) (a) Wang, K.; Cai, X.; Yao, W.; Tang, D.; Kataria, R.; Ashbaugh, H. S.; Byers, L. D.; Gibb, B. C. Electrostatic Control of Macrocyclization Reactions within Nanospaces. *J. Am. Chem. Soc.* **2019**, *141*,

https://doi.org/10.26434/chemrxiv-2024-4w50c-v2 **ORCID:** https://orcid.org/0000-0003-0035-4565 Content not peer-reviewed by ChemRxiv. **License:** CC BY-NC-ND 4.0

6740 – 6747. doi.org/10.1021/jacs.9b02287. (b) Cai, X.; Kataria, R.; Gibb, B. C. Intrinsic and Extrinsic Control of the pK_a of Thiol Guests Inside Yoctoliter Containers. *J. Am. Chem Soc.* **2020**, *142*, 8291 – 8298. doi.org/10.1021/jacs.0c00907. (c) Zhang, Q.; Tiefenbacher, K. Terpene Cyclization Catalyzed Inside a Self-Assembled Cavity. *Nat. Chem.* **2015**, *7*, 197 – 202. doi.org/10.1038/nchem.2181.

(8) (a) Száraz, S.; Oesterhelt, D.; Ormos, P. pH-induced structural changes in bacteriorhodopsin studied by Fourier transform infrared spectroscopy. *Biophys. J.* **1994**, *57*, 1706 – 1712. doi.org/10.1016/S0006-3495(94)80644-7. (b) Luecke, H.; Richter, H.-T.; Lanyi, J. K. Proton Transfer Pathways in Bacteriorhodopsin at 2.3 Angstrom Resolution. *Science* **1998**, *280*, 1934 – 1937. doi.org/10.1126/science.280.5371.1934.

(9) (a) Karp, D. A.; Gittis, A. G.; Stahley, M. R.; Fitch, C. A.; Stites, W. E.; García-Moreno, E. B. High Apparent Dielectric Constant Inside a Protein Reflects Structural Reorganization Coupled to the Ionization of an Internal Asp. *Biophys. J.* **2007**, *92*, 2041 – 2053. doi.org/10.1529/biophysj.106.090266. (b) Harms, M. J.; Castañeda, C. A.; Schlessman, J. L.; Sue, G. R.; Isom, D. G.; Cannon, B. R.; García-Moreno, E. B. The p*K*a Values of Acidic and Basic Residues Buried at the Same Internal Location in a Protein Are Governed by Different Factors. *J. Mol. Biol.* **2009**, *389*, 34 – 47. doi.org/10.1016/j.jmb.2009.03.039. (c) Grimsley, G. R.; Scholtz, J. M.; Pace, C. N. A summary of the measured pK values of the ionizable groups in folded proteins. *Protein Sci.* **2009**, *18*, 247 – 251. doi.org/10.1002/pro.19. (d) Awoonor-Williams, E.; Golosov, A. A.; Hornak, V. Benchmarking *In Silico* Tools for Cysteine p*K*a Prediction. *J. Chem. Inf. Model.* **2023**, *63*, 2170 – 2180. doi.org/10.1021/acs.jcim.3c00004.

(10) (a) Cook, T. R.; Stang, P. J. Recent Developments in the Preparation and Chemistry of Metallacycles and Metallacages via Coordination. *Chem. Rev.* **2015**, *115*, 7001 – 7045. doi.org/10.1021/cr5005666. (b) Durot, S.; Taesch, J.; Heitz, V. Multiporphyrinic Cages: Architectures and Functions. *Chem. Rev.* **2014**, *114*, 8542– 8578. doi.org/10.1021/cr400673y. (c) Fujita, N.; Biradha, K.; Fujita, M.; Sakamoto, S.; Yamaguchi, K. A Porphyrin Prism: Structural Switching Triggered by Guest Inclusion. *Angew. Chem., Int. Ed.* **2001**, *40*, 1718−1721. doi.org/10.1002/1521-3773(20010504)40:9%3C1718::AID-ANIE17180%3E3.0.CO;2-7. (d) Bar, A. K.; Mohapatra, S.; Zangrando, E.; Mukherjee, P. S. A Series of Trifacial Pd_6 Molecular Barrels with Porphyrin Walls. *Chem. Eur. J.* **2012**, *18*, 9571–9579. doi.org/10.1002/chem.201201077.

(11) (a) Dutton, K. G.; Rothschild, D. A.; Pastore, D. B.; Emge, T. J.; Lipke, M. C. The Influence of Redox-Active Linkers on the Stability and Physical Properties of a Highly Electroactive Porphyrin Nanoprism. *Inorg. Chem.* **2020**, *59*, 12616–12624, doi.org/10.1021/acs.inorgchem.0c01719. (b) Mansoor, Iram F.; Dutton, K. G.; Rothschild, D. A.; Remsing, R. C.; Lipke, M. C. Uptake, Trapping, and Release of Organometallic Cations by Redox-Active Cationic Hosts. *J. Am. Chem. Soc.* **2021**, *143*, 16993 – 17003. doi.org/10.1021/jacs.1c06121. (c) Blackburn, P. Thomas; Mansoor, Iram F.; Dutton, Kaitlyn G.; Tyryshkin, Alexei M.; Lipke, Mark C. Accessing three oxidation states of cobalt in M_6L_3 nanoprisms with cobalt–porphyrin walls. *Chem. Commun.* **2021**, *57*, 11342 – 11345. doi.org/10.1039/D1CC04860K. (d) Dutton, K. G.; Jones, T. J.; Emge, T. J.; Lipke, M. C. Cage Match: Comparing the Anion Binding Ability of Isostructural Versus Isofunctional Pairs of Metal-Organic Nanocages. *Chem. Eur. J.* **2024**, *30*, e202303013. doi.org/10.1002/chem.202303013. (e) Blackburn, P. Thomas; Lipke, Mark C. Effects of a triangular nanocage structure on the binding of neutral and anionic ligands to Co^{II} and Zn^{II} porphyrins. *J. Coord. Chem.* **2022**, *75*, 1520 – 1542. doi.org/10.1080/00958972.2022.2128786.

(12) (a) Smith, P. T.; Benke, B. P.; Cao, Z.; Kim, Y.; Nichols, E. M.; Kim, K.; Chang, C. J. Iron Porphyrins Embedded into a Supramolecular Porous Organic Cage for Electrochemical CO_2 Reduction in Water. *Angew. Chem., Int. Ed.* **2018**, *57*, 6984 – 6988. doi.org/10.1002/anie.201803873. (b) Smith, P. T.; Kim, Y.; Benke, B. P.; Kim, K.; Chang, C. J. Supramolecular Tuning Enables Selective Oxygen Reduction Catalyzed by Cobalt Porphyrins for Direct Electrosynthesis of Hydrogen Peroxide. *Angew. Chem., Int. Ed.* **2020**, *59*, 4902 – 4907. doi.org/10.1002/anie.201916131. (c) Oldacre, A. N.; Friedman, A. E.; Cook, T. R. A Self-Assembled Cofacial Cobalt Porphyrin Prism for Oxygen Reduction Catalysis. *J. Am. Chem. Soc.* **2017**, *139*, 1424 – 1427. doi.org/10.1021/jacs.6b12404. (d) Crawley, M. R.; Zhang, D.; Oldacre, A. N.; Beavers, C. M.; Friedman, A. E.; Cook, T. R. Tuning the Reactivity of Cofacial Porphyrin Prisms for Oxygen Reduction Using Modular Building Blocks. *J. Am. Chem. Soc.* **2021**, *143*, 1098 – 1106. doi.org/10.1021/jacs.0c11895. (e) Crawley, M. R.; Zhang, D.; Cook, T. R. Electrocatalytic production of hydrogen peroxide enabled by post-synthetic modification of a self-assembled porphyrin cube. *Inorg. Chem. Front.* **2023**, *10*, 316 – 324. doi.org/10.1039/D2QI02050E. (f) Nurttila, S. S.; Zaffaroni, R.; Mathew, S.; Reek, J. N. H. Control of the overpotential of a [FeFe] hydrogenase mimic by a synthetic second coordination sphere. *Chem. Commun.* **2019**, *55*, 3081 – 3084. doi.org/10.1039/C9CC00901A.

(13) (a) Lin, S.; Diercks, C. S.; Zhang, Y.-B.; Kornienko, N.; Nichols, E. M; Zhao, Y.; Paris, A. R.; Kim, D.; Yang, P.; Yaghi, O. M.; Chang, C. J. Covalent organic frameworks comprising cobalt porphyrins for catalytic CO_2 reduction in water. *Science* **2015**, *349*, 1208 – 1213. doi.org/10.1126/science.aac8343. (b) Kornienko, N.; Zhao, Y.; Kley, C. S.; Zhu, C.; Kim, D.; Lin, S.; Chang, C. J.; Yaghi, O. M.; Yang, P. Metal–Organic Frameworks for Electrocatalytic Reduction of Carbon Dioxide. *J. Am. Chem. Soc.* **2015**, *137*, 14129 – 14135. doi.org/10.1021/jacs.5b08212. (c) Liberman, I.; Shimoni, R.; Ifraemov, R.; Rozenberg, I.; Singh, C.; Hod I. Active-Site Modulation in an Fe-Porphyrin-Based Metal–Organic Framework through Ligand Axial Coordination: Accelerating Electrocatalysis and Charge-Transport Kinetics. *J. Am. Chem. Soc.* **2020**, *142*, 1933 – 1940. doi.org/10.1021/jacs.9b11355. (d) Shimoni, R.; Shi, Z.; Binyamin, S.; Yang, Y.; Liberman, I.; Ifraemov, R.; Mukhopadhyay, S.; Zhang, L.; Hod, I. Electrostatic Secondary-Sphere Interactions That Facilitate Rapid and Selective Electrocatalytic CO2 Reduction in a Fe-Porphyrin-Based Metal–Organic Framework. *Angew. Chem., Int. Ed.* **2022**, *61*, e202206085. doi.org/10.1002/anie.202206085. (e) Gong, L.; Chen, B.; Gao, Y.; Yu, B.; Wang, Y.; Han, B.; Lin, C.; Bian, Y.; Qi, D.; Jiang, J. Covalent organic frameworks based on tetraphenyl-p-phenylenediamine and metalloporphyrin for electrochemical conversion of CO2 to CO. *Inorg. Chem. Front.* **2022**, *9*, 3217 – 3223. doi.org/10.1039/D2QI00336H. (f) Wu, Q.-J.; Si, D.-H.; Wu, Q.; Dong, Y.-L.; Cao, R.; Huang, Y.-B. Boosting Electroreduction of CO2 over Cationic Covalent Organic Frameworks: Hydrogen Bonding Effects of Halogen Ions. *Angew. Chem., Int. Ed.* **2023**, *62*, e202215687. doi.org/10.1002/anie.202215687.

(14) (a) Teinl, K.; Patrick, B. O.; Nichols, E. M. Linear Free Energy Relationships and Transition State Analysis of CO_2 Reduction Catalysts Bearing Second Coordination Spheres with Tunable Acidity. *J. Am. Chem. Soc.* **2023**, *145*, 31, 17176 – 17186. doi.org/10.1021/jacs.3c03919. (b) Sonea, A.; Crudo, N. R.; Warren, J. J. Understanding the Interplay of the Brønsted Acidity of Catalyst Ancillary Groups and the Solution Components in Iron-porphyrin-Mediated Carbon Dioxide Reduction. *J. Am. Chem. Soc.* **2024**, *146*, 3721–3731. doi.org/10.1021/jacs.3c10127. (c) Yeh, C.-Y.; Chang, C. J.; Nocera, D. G. "Hangman" Porphyrins for the Assembly of a Model Heme Water Channel. *J. Am. Chem. Soc.* **2001**, *7*, 1513 – 1514. doi.org/10.1021/ja003245k. (d) Bediako, D. K.; Solis, B. H.; Dogutan, D. K.; Roubelakis, M. M.; Maher, A. G.; Lee, C. H.; Chambers, M. B.; Hammes-Schiffer, S.; Nocera, D. G. Role of pendant proton relays and proton-coupled electron transfer on the hydrogen evolution reaction by nickel hangman porphyrins. *Proc. Natl. Acad. Sci. USA* **2014**, *111*, 15001 – 15006. doi.org/10.1073/pnas.1414908111.

(15) To our knowledge, the largest changes of acidity measured in proteins are $\Delta pK_a \approx 8.5$ (see references 8a, 9c, and 9d), while pK_a changes of ≤ 6 are more common in both proteins and artificial nanocages (see references 3b-e, 4b-d, 5b-c, 6, 7a, 7b, and 9).

https://doi.org/10.26434/chemrxiv-2024-4w50c-v2 **ORCID:** https://orcid.org/0000-0003-0035-4565 Content not peer-reviewed by ChemRxiv. **License:** CC BY-NC-ND 4.0

(16) Craen, D. V.; Kalarikkal, M. G.; Holstein, J. J. A Charge-Neutral Self-Assembled L_2Zn_2 Helicate as Bench-Stable Receptor for Anion Recognition at Nanomolar Concentration. *J. Am. Chem. Soc.* **2022**, 144, 18135 – 18143. doi.org/10.1021/jacs.2c08579.

(17) Bryant, R. G. The NMR time scale. *J. Chem. Educ.* **1983**, *60*, 933 – 935. doi.org/10.1021/ed060p933.

(18) $^{13}C\{^1H\}$ NMR and 2D NMR experiments were used to confirm the assignments of the signals of the $\mathbf{1_A}^-$ guests in the TriCages. These experiments required high sample concentrations and the use of non-routine (700 MHz) NMR instrumentation, which was prohibitive for characterizing all the complexes, so **(1A⁻)₂@Zn₃TriCage** was selected for representative characterization (see Figures S39 – S43). The chemical shifts of the ^1H NMR signals of the guest are similar to those reported for *p*-tolylSO_3^- in **TriCage** (reference 11d), which has the CH_3 group placed near the center of the host.

(19) (a) Tshepelevitsh, S.; Kütt, A.; Lõkov, M.; Kalijurand, I.; Saame, J.; Heering, A.; Plieger, P. G.; Vianello, R.; Leito, I. On the Basicity of Organic Bases in Different Media. *Eur. J. Org. Chem.* **2019**, *2019*, 6735 – 6748. doi.org/10.1002/ejoc.201900956. (b) Kütt, A.; Tshepelevitsh, S.; Saame, J.; Lõkov, M.; Kalijurand, I.; Selberg, S.; Leito, I. Strengths of Acids in Acetonitrile. *Eur. J. Org. Chem.* **2021**, *2021*, 1407 – 1419. doi.org/10.1002/ejoc.202001649. (c) Kaupmees, K.; Kalijurand, I.; Leito, I. Influence of Water Content on the Acidities in Acetonitrile. Quantifying Charge Delocalization in Anions. *J. Phys. Chem. A* **2010**, *114*, 11788 – 11793. doi.org/10.1021/jp105670t.

(20) (a) Patrick, S. C.; Beer, P. D.; Davis, J. J. Solvent effects in anion recognition. *Nat. Rev. Chem.* **2024**, *8*, 256 – 276. (b) Sokkalingam, P.; Shraberg, J.; Rick, S. W.; Gibb, B. C. Binding Hydrated Anions with Hydrophobic Pockets. *J. Am. Chem. Soc.* **2016**, *138*, 48 – 51. doi.org/10.1021/jacs.5b10937.

(21) Fourmond, V.; Jacques, P.-A.; Fontecave, M.; Artero, V. H_2 Evolution and Molecular Electrocatalysts: Determination of Overpotentials and Effect of Homoconjugation. *Inorg. Chem.* **2010**, *49*, 10338 – 10347. doi.org/10.1021/ic101187v.

(22) Traces of water can have relatively large effects on increasing the acidity of benzoic acids in MeCN (see reference 19c), so it is worth noting that our measured pK_a (20.75 ± 0.04) for 4-sulfanatobenzoic acid ($\mathbf{1_A}^-$) is reasonable based on the known acidity of benzoic acid in MeCN (pK_a = 21.5, reference 19b) and the positive σ_p Hammett parameter for SO_3^- (reference 23). Additionally, even a somewhat large systematic error (≤1.5 pK_a units) in the acidity of $\mathbf{1_A}^-$ measured in bulk MeCN would not affect our conclusions about the relative contributions of different factors that influence the acidity of this guest inside the **M_3TriCages**.

(23) Hansch, C.; Leo, A.; Taft, R. W. A Survey of Hammett Substituent Constants and Resonance and Field Parameters. *Chem. Rev.* **1991**, *91*, 165 – 195. doi.org/10.1021/cr00002a004.

(24) A statistical correction of +0.3 units should be applied to the pK_a of **$(\mathbf{1_A}^-)_2$@Co_3TriCage** when comparing the acidity of this diprotic complex with that of the monoprotic complex **$\mathbf{1_A}^-$@Co_3TriCage**. Thus, the acidity of the latter complex relative to the former is appropriately estimated as $\Delta pK_a \leq -0.83 \pm 0.16$.

(25) The acidities of **$(\mathbf{1_A}^-)_2$@Co_3TriCage** under hydrated vs. anhydrous conditions are not statistically distinguishable based on direct pK_a measurements, but the stronger interactions of water with **$(\mathbf{1_A}^-)_2$@Co_3TriCage** vs. **$(\mathbf{1_A}^-)(\mathbf{1_B}^{2-})$@$Co_3$TriCage** make it clear that the hydrated state of the diprotic complex must be at least slightly less acidic than its anhydrous state.

(26) Agarwal, R. G.; Coste, S. C.; Groff, B. D.; Heuer, A. M.; Noh, H.; Parada, G. A.; Wise, C. F.; Nichols, E. M.; Warren, J. J.; Mayer, J. M. Free Energies of Proton-Coupled Electron Transfer Reagents and Their Applications. *Chem. Rev.* **2022**, *122*, 1 – 49. doi.org/10.1021/acs.chemrev.1c00521.

(27) The strength of $CO_2^- \rightarrow Co^{II}$ coordination in anhydrous **$\mathbf{1_B}^{2-}$@Co_3TriCage** was determined to be ca. 4 kcal mol⁻ based on comparisons of pK_a values that indicate an enhancement of stability of the dianion by ~2.3 kcal mol⁻ in this complex relative to **$(\mathbf{1_A}^-)(\mathbf{1_B}^{2-})$@TriCage**, and the estimate that **$\mathbf{1_A}^-$---$\mathbf{1_B}^{2-}$** hydrogen bonding stabilizes the latter complex by ~1.5 kcal mol⁻.

(28) (a) Becke, A. D. Density-Functional Exchange-Energy Approximation with Correct Asymptotic Behavior. *Phys. Rev. A*, **1988**, *38*, 3098-3100, doi.org/10.1103/PhysRevA.38.3098. (b) Lee, C. T.; Yang, W. T.; Parr, R. G. Development of the Colle-Salvetti Correlation-Energy Formula into a Functional of the Electron Density. *Phys. Rev. B*, **1988**, *37*, 785–789. doi.org/10.1103/PhysRevB.37.785.

(29) (a) Petersson, G. A.; Al-Laham, M. L. A complete basis set model chemistry. II. Open-shell systems and the total energies of the first-row atoms. *J. Chem. Phys.*, **1991**, *94*, 6081–6090. doi.org/10.1063/1.460447. (b) Hay, P. J.; Wadt, W. R. *Ab initio* effective core potentials for molecular calculations – potentials for the transition-metal atoms Sc to Hg. *J. Chem. Phys.*, **1985**, *82*, 270-283. doi.org/10.1063/1.448799.

(30) (a) Shen, J.; Kolb, M. J.; Göttle, A. J.; Koper, M. T. DFT Study on the Mechanism of the Electrochemical Reduction of CO_2 Catalyzed by Cobalt Porphyrins. *J. Phys. Chem. C* **2016**, *120*, 15714 – 15721. doi.org/10.1021/acs.jpcc.5b10763. (b) Zhu, C.; D'Agostino, C.; de Visser, S. P. CO_2 Reduction by an Iron(I) Porphyrinate System: Effect of Hydrogen Bonding on the Second Coordination Sphere. *Inorg. Chem.* **2024**, *63*, 4474 – 4481. doi.org/10.1021/acs.inorgchem.3c04246.

(31) (a) Can, M.; Armstrong, F. A.; Ragsdale, S. W. Structure, Function, and Mechanism of the Nickel Metalloenzymes, CO Dehydrogenase, and Acetyl-CoA Synthase. *Chem. Rev.* **2014**, *114*, 4149 – 4174. doi.org/10.1021/cr400461p. (b) Hussein, R.; Graca, A.; Forsman, J.; Aydin, A. O.; Hall, M.; Gaetcke, J.; Chernev, P.; Wendler, P.; Dobbek, H.; Messinger, J.; Zouni, A.; Schröder, W. P. Cryo-electron microscopy reveals hydrogen positions and water networks in photosystem II. *Science* **2024**, *384*, 1349 – 1355. doi.org/10.1126/science.adn6541. (c) Hart-Cooper, W. M.; Sgarlata, C.; Perrin, C. L.; Toste, F. D.; Bergman, R. G.; Raymond, K. N. Protein-like proton exchange in a synthetic host cavity. *Proc. Natl. Acad. Sci. USA* **2015**, *112*, 15303 – 15307. doi.org/10.1073/pnas.1515639112.

https://doi.org/10.26434/chemrxiv-2024-4w50c-v2 **ORCID:** https://orcid.org/0000-0003-0035-4565 Content not peer-reviewed by ChemRxiv. **License:** CC BY-NC-ND 4.0

TOC Graphic

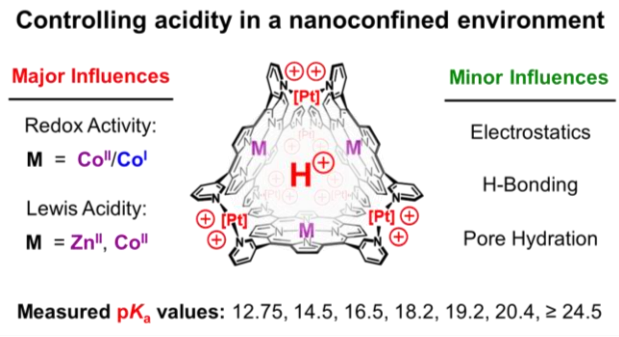

https://doi.org/10.26434/chemrxiv-2024-4w50c-v2 **ORCID:** https://orcid.org/0000-0003-0035-4565 Content not peer-reviewed by ChemRxiv. **License:** CC BY-NC-ND 4.0